Environ. Sci. Technol. **2006**, *40,* 5763−5769

High Temporal Resolution Oxygen Imaging in Bioirrigated Sediments

LUBOS POLERECKY,*,† NILS VOLKENBORN,‡ AND PETER STIEF†,§

Max-Planck-Institute for Marine Microbiology, Celsiusstrasse 1, 28359, Bremen, Germany, Alfred-Wegener-Institute for Polar and Marine Research, Wadden Sea Station Sylt, Hafenstrasse 43, 25992, List, Germany

A technique is presented for temporal characterization of the bioirrigation activity of benthic macrofauna and for quantitative estimation of its effects on the oxygen exchange between the sediment and the overlying water. The technique is based on high temporal resolution (15−30 s) oxygen imaging aided by a planar oxygen optode and can be applied under laboratory and field conditions, both freshwater and marine. It allows direct observation of the complex 2D oxygen dynamics in the sediment around the burrow while the animal dwells undisturbed in its natural environment. The conditions to which the animal is exposed can easily be controlled or manipulated. *Chironomus plumosus*, widely distributed freshwater insect larvae, were used in a case study. Their bioirrigation activity was divided into a random succession of pumping intervals (duration 5.4 ± 1.7 min) and rest periods (duration 9.2 ± 5.8 min). The burrow ventilation resulted in a highly variable volume of the oxygenated sediment surrounding the burrow and the associated sedimentary oxygen uptake rate through the burrow wall (OUB), both changing dramatically within minutes. Their variability was higher in a burrow under construction than around a stationary burrow. The average OUB rate (∼0.15 μmol O_2 h^{-1}), when translated into a time-averaged O_2 flux across the burrow wall, constituted approximately 64% of the stationary diffusive oxygen flux measured at the sediment−water interface (∼0.9 mmol O_2 m^{-2} h^{-1}).

Introduction

Active ventilation of animal burrows, i.e., bioirrigation, is a widespread phenomenon in aquatic sediments. Burrow ventilation with overlying water provides oxygen for animal respiration and serves, in the case of filter feeders, as a means of collecting food. By creating burrows and pumping water through them, benthic macrofauna increase the effective sediment surface area (*1*,*2*) and thus significantly influence the overall exchange of solutes (e.g., oxygen, nutrients) between the sediment and the overlying water (*3*−*6*). Bioirrigating animals thus benefit not only themselves, but also turn the sediment surrounding the burrows into a habitat suitable for diverse microbial and meiobenthic populations (*7*−*11*).

* Corresponding author phone: 0049-421-2028 834; fax: 0049-421-2028 690; e-mail: lpolerec@mpi-bremen.de.
† Max-Planck-Institute for Marine Microbiology.
‡ Alfred-Wegener-Institute for Polar and Marine Research.
§ Present address: Aarhus University, Department of Microbiology, Ny Munkegade, Building 540, DK-8000 Aarhus C, Denmark.

High spatial resolution techniques revealed a complex oxic−anoxic mosaic inside aquatic sediments inhabited by bioirrigating organisms. For example, in-situ oxygen microsensor measurements demonstrated the enhanced delivery of oxygen into the sediment due to bioirrigation by showing the presence of suboxic regions several cm below the sediment surface in an otherwise anoxic sediment and/or by observing a significantly deeper oxygen penetration into the sediment (e.g., refs *10*, *12*−*17*). Even though microsensor measurements provide a useful indication of the presence or absence of bioirrigation, their use in the direct quantification of the effects on oxygen exchange is limited, mainly due to the 1D character and low temporal resolution of the measured profiles.

A more complex and illuminating picture of the effects of bioirrigating macrofauna on the oxygen distribution in the sediment was revealed by in-situ planar optode based oxygen imaging (*15*, *18*). However, heat dissipation and limited power supply of the in-situ module constrains the temporal resolution of the images to 10−30 min, which is insufficient to adequately capture the true oxygen dynamics in the sediment surrounding the ventilated burrow (*19*, *20*). Therefore, this technology alone cannot be used to quantify the temporal variability of the bioirrigation activity nor its effects on the oxygen exchange between the sediment and the overlying water.

The standard approach for the quantification of the sediment−water oxygen exchange employs the measurement of oxygen decrease inside an intact sediment enclosure, either in the laboratory or in situ (e.g., refs *20*−*24*). However, such measurements provide little information about the mechanisms underlying the oxygen consumption or production, mainly due to the lack of the necessary high spatial resolution. The approach where the chamber measurements are combined with the microsensor and/or planar optode data is, therefore, optimal to elucidate the oxygen exchange processes associated with bioirrigation (*15*).

Here we present planar optode based laboratory measurements of oxygen dynamics in the sediment around ventilated burrows of *Chironomus plumosus* larvae. We show that tens of seconds is the temporal resolution required to capture the dynamics adequately. Using a simplified model, we describe how such high temporal resolution series of 2D oxygen distributions can be used to (i) quantify the sediment volume oxygenated by burrow ventilation, (ii) estimate the associated enhancement of the sedimentary oxygen uptake without losing the information about the governing mechanism, and (iii) analyze the temporal patterns in macrofaunal pumping activity in its natural environment. We highlight the possibilities offered by the planar optode technique, but also critically assess its limitations in the study of bioirrigation.

Experimental Section

Chironomus plumosus larvae and the sediment were collected from Grosser Binnensee, a freshwater lake in North Germany. The worm-shaped larvae were approximately 20 mm long and 2 mm in diameter. The sediment (water content 86%, organic matter content 15%, grain size distribution not available) was defaunated by sieving through a 1 mm mesh and homogenized.

The two-dimensional (2D) oxygen distributions were measured using the laboratory based luminescence lifetime imaging system (*25*−*28*) and a semitransparent planar oxygen optode. The optode, prepared as described previously (*26*), was attached to a transparent polycarbonate window of an aquarium. The aquarium was filled with the sediment and

10.1021/es060494l CCC: $33.50
Published on Web 08/10/2006

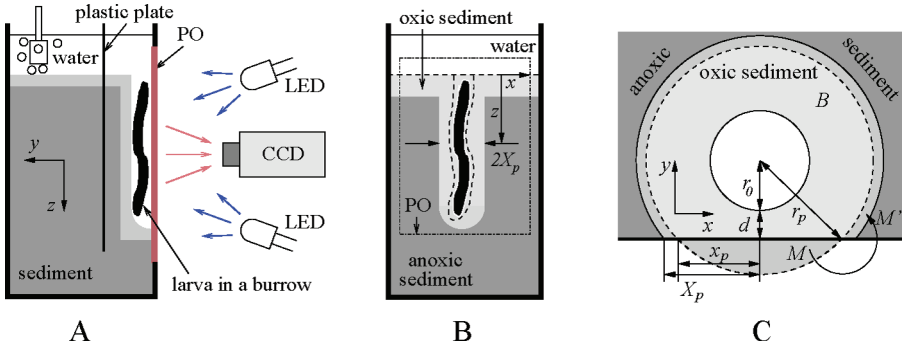

FIGURE 1. (A) Side and (B) front views of the experimental arrangement. Luminescence of the oxygen sensitive indicator dye, which is embedded in the polymer matrix of the planar optode (PO), is excited by blue light emitting diodes (LEDs) and detected by a fast gateable CCD camera. (C) Horizontal cross section of a cylindrical burrow located at distance *d* from a wall (e.g., a PO). Area of the oxic sediment around the burrow was approximated by the sum of area *B* (light gray) and the area of the "missing sediment" (middle gray, *M* = *M'*). Area *B* (with radius r_p) corresponds to the axially symmetric situation without the wall present. As a consequence, the extent of oxygen at the wall (X_p) is greater than the radial oxygen penetration (r_p) projected to the plane of the wall (x_p). Note that the larva and the burrow are not drawn to scale in this schematic.

covered with tap water of similar chemical composition as the lake water (moderate conductivity, circumneutral pH, low nutrient content). A thin, flat plastic plate was subsequently inserted into the sediment approximately 2 cm away from the optode to restrict the space where the benthic macrofauna could dwell (Figure 1A−B). The conditions were allowed to settle for 3 days, with the overlying water being bubbled with air.

Before the addition of *C. plumosus*, several vertical oxygen microprofiles at random horizontal positions over the sediment surface were measured using a Clark-type microelectrode (*29*) until a steady state in O_2 distribution was reached. These profiles as well as the profiles extracted from the steady-state oxygen images were used to calculate the diffusive flux in the diffusive boundary layer. The average volumetric oxygen uptake rates of the top sediment layer were then calculated by dividing the fluxes by the corresponding oxygen penetration depths.

Following these initial measurements, several *C. plumosus* larvae were introduced on top of the sediment in the space between the planar optode and the plastic plate. Oxygen imaging in 15−30 s intervals was started immediately afterward. Imaging was conducted in the dark to avoid possible influence of the ambient light on the luminescence-based measurements and on the oxygen distribution in the sediment (e.g., due to primary production). The overlying water was aerated and the temperature was kept constant at 18 °C during all measurements. The images presented below, as well as movies provided as Supporting Information, are representative of at least five serially conducted recordings.

Basic Theory. After the aerated water is pumped into the burrow, oxygen is transported into the surrounding sediment, where it is consumed due to microbial respiration and/or chemical oxidation of reduced compounds. If the local volumetric sedimentary consumption rate (R in mol m^{-3} s^{-1}) is known, the rate of oxygen uptake around the burrow (*OUB* in mol s^{-1}) is

$$\mathrm{OUB}(t) = \int_{V(t)} R\, dV \qquad (1)$$

where $V(t)$ is the time-variable volume of the oxygenated sediment. Approximating the burrow by a cylinder of radius r_0 and length L, neglecting the edge effects at both cylinder ends and assuming a variable radius of oxygen penetration r_p, $V(t)$ can be written as

$$V(t) \approx \int_0^L A_{oxic}(z;t)\, dz \qquad (2)$$

where A_{oxic} is the cross-section area of the oxygenated sediment and z denotes the depth coordinate (Figure 1C). In the absence of the planar optode, A_{oxic} is simply equal to $\pi(r_p^2 - r_0^2)$, where r_p varies with time. However, when the planar optode is near the burrow wall, an exact formula for A_{oxic} cannot be found analytically. To provide an approximation for $V(t)$ without the need of extensive numerical simulations, the effect of the planar optode on the actual time-dependent oxygen distribution around the burrow was neglected. Instead, it was assumed that the "missing" sediment in front of the optode (area M in Figure 1C) that should be contributing to oxygen consumption was substituted by sediment around the burrow with volume equivalent to that cut off by the optode (area M' in Figure 1C). This substitution led to an apparent increase of the oxygen penetration depth at the position of the planar optode from x_p to X_p, but to no change in the sedimentary oxygen consumption capacity. Consequently, the relation between A_{oxic} and the extent of oxygen observed by the planar optode, X_p, can be written explicitly as

$$A_{oxic}(z;t) = B + M - \pi r_0^2 = (r_0 + d)X_p - \pi r_0^2 + [(r_0 + d)^2 + X_p^2][\pi - \arctan(X_p/(r_0 + d))] \qquad (3)$$

where d is the distance between the burrow wall and the planar optode (Figure 1C). Thus, the enhancement of the total sedimentary uptake rate due to the penetration of oxygen into the sediment surrounding the burrow can be estimated by (i) calculating the depth-dependent area $A_{oxic}(z;t)$ from the extent of oxygen measured by the planar optode (eq 3), and (ii) integrating this area over the observed burrow length (eq 2) and integrating the local consumption rate over the volume of the oxic sediment (eq 1).

The local consumption rate around the burrow, R, was evaluated from the measured time series of 2D oxygen distributions (27, 28). Assuming diffusive transport, the concentration change observed by the planar optode is described by the time-dependent diffusion equation $\partial c/\partial t = D_s(\partial^2 c/\partial x^2 + \partial^2 c/\partial y^2 + \partial^2 c/\partial z^2) - R$, where D_s is the diffusion coefficient. The term $\partial^2 c/\partial z^2$ could be neglected since the observed concentration gradients varied in the z direction much less than in the x direction (i.e., $\partial^2 c/\partial z^2 \ll \partial^2 c/\partial x^2$). Since the concentration profile in the y direction cannot be measured by the planar optode (Figure 1C), the term $\partial^2 c/\partial y^2$ remained unknown. The values of R were subsequently calculated as

$$R \approx D_s \partial^2 c/\partial x^2 - \partial c/\partial t \qquad (4)$$

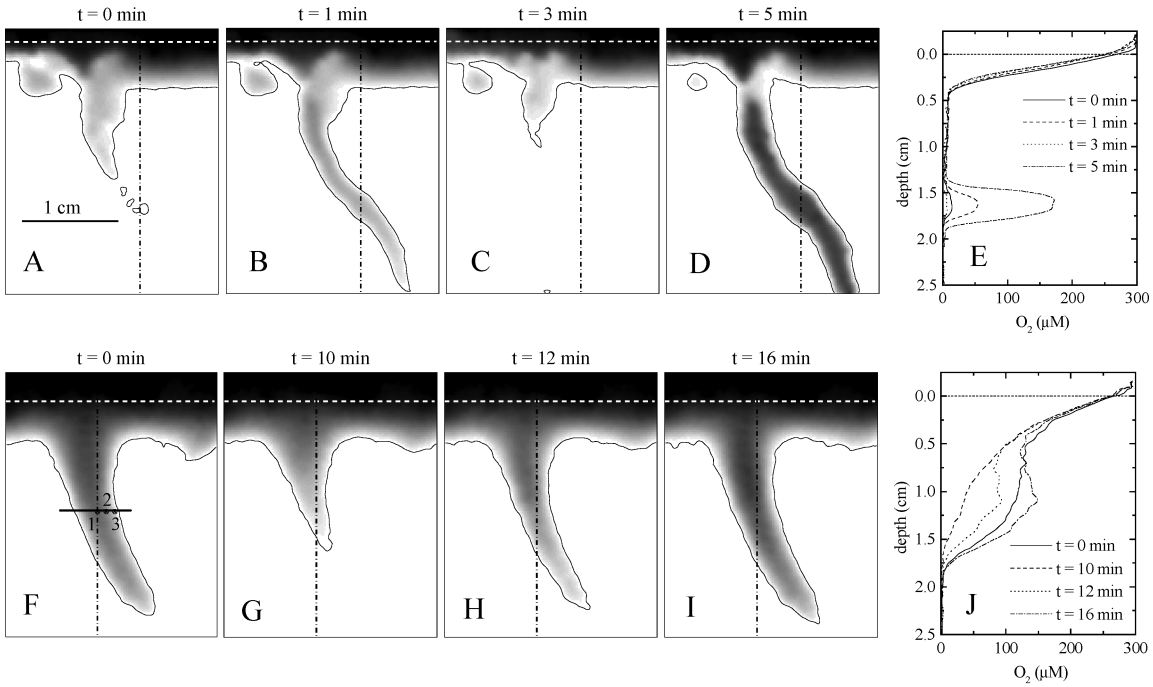

FIGURE 2. Selected oxygen images and the corresponding 1D vertical profiles taken during the construction of a burrow (A−E) and around a stationary burrow (different one) with a larva dwelling in it (F−J). The vertical profiles were extracted from the images at the location indicated by the dash−dotted line. Dashed horizontal line indicates an approximate location of the sediment surface, black solid line indicates the boundary between oxic and anoxic sediment. Videos of the complete time series are available as Supporting Information. Time in the videos is displayed in the format hh:mm:ss.

bearing in mind that they could possibly be under/overestimated due to the neglect of the $\partial^2 c/\partial y^2$ term. The pixel-wise determination of the term $\partial c/\partial t$ was done using the algorithm described previously (*27*). The effect of diffusion ($D_s\partial^2 c/\partial x^2$) was determined by fitting the horizontal profile extracted from the oxygen image and taking the second derivative of the fit. The diffusion coefficient was calculated as $D_s = (\phi/\theta^2)D_w$, taking into account the sediment porosity (ϕ) and tortuosity ($\theta^2 = 1 - \ln(\phi^2)$) (*30*) and the oxygen diffusion coefficient in water (D_w) corrected for temperature and salinity (*31*).

Results

Immediately after the placement on the sediment surface, the larvae started to create new burrows in the sediment, which they later inhabited. If the burrow was created sufficiently close to it (Figure 1A−B), the effects of the burrow flushing with the overlying water were directly observed by the planar optode as oxic plumes along the burrow (Figure 2A−D and F−I). The measured O_2 images as well as the vertical profiles extracted from them (Figure 2E and J) show similar features as those obtained in-situ (*12*, *14*−*18*). The analysis of hundreds of oxygen images shows, however, that the volume of the oxygenated sediment around the ventilated burrow is highly variable and can change very rapidly, within minutes or even seconds. This suggests that the 1D microprofiles and/or the 2D images presented previously should be considered as snapshots that may not necessarily represent a typical or average situation.

The burrows were ventilated in a sequence of pumping events (PE's) followed by periods of rest (RP's), as interpreted from the temporal variation of the oxygen concentrations in selected pixels (Figure 3A−B). The time interval between the start of the oxygen increase and the moment it reached maximum (t_{max} in Figure 3B) was considered as the duration of the PE (T_{PE}), whereas the interval between t_{max} and the start of the subsequent oxygen increase was taken as the RP duration (T_{RP}). PE durations were shorter and less variable than the RP durations, with the average and standard deviations of $T_{PE} = 5.4 \pm 1.7$ min and $T_{RP} = 9.2 \pm 5.8$ min (Figure 3C). No correlation between T_{RP}'s and the previous/subsequent T_{PE}'s was found (regression analysis: $R_{prev} = 0.097$; $p = 0.45$; $R_{subs} = 0.196$; $p = 0.13$), nor was there any correlation between the durations of the subsequent PEs ($R = 0.09$; $p = 0.49$) and RPs ($R = 0.05$; $p = 0.70$). The Kolmogorov−Smirnov test revealed that both T_{PE} and T_{RP} could best be characterized by a log-normal distribution ($d_{PE} = 0.074$, $d_{RP} = 0.110$), indicating that both periods have a characteristic duration but both can occasionally last much longer (Figure 3C).

When the rest periods were sufficiently long, O_2 concentrations decreased with approximately a constant rate (Figure 3B), which was reproducible over RP's of similar duration (e.g., $\partial c/\partial t = -90 \pm 14$ μmol m^{-3} s^{-1} for curve 1). The rates were lower in pixels selected further away from the center of the oxic plume (compare the linear approximations L_1−L_3 in Figure 3B). This effect was identified as the influence of diffusion on the O_2 dynamics (eq 4), whereby the positive and negative second derivatives of the horizontal O_2 profile in points 3 and 1 (Figure 4A) resulted, respectively, in reduced and enhanced rates of the concentration decrease in these points compared to point 2. Another possibility would be the lower sedimentary O_2 uptake rates, R, at lower O_2 concentrations, but this was not considered as it could not be resolved from our data. Using eq 4, local sedimentary uptake rates of $R = 52$−73 μmol m^{-3} s^{-1} were determined. These rates were similar but somewhat lower than the average rates of 80−90 μmol m^{-3} s^{-1} determined from the diffusive fluxes (0.24−0.27 μmol m^{-2} s^{-1}) and the average oxygen penetration depth (3.0 mm) measured at the undisturbed sediment surface (profiles not shown).

Horizontal oxygen profiles around the burrow exhibited similar patterns regarding their temporal variation as the concentration dynamics in selected pixels (Figure 4). However, the extent of oxygen at the wall (X_p, Figure 1C) varied

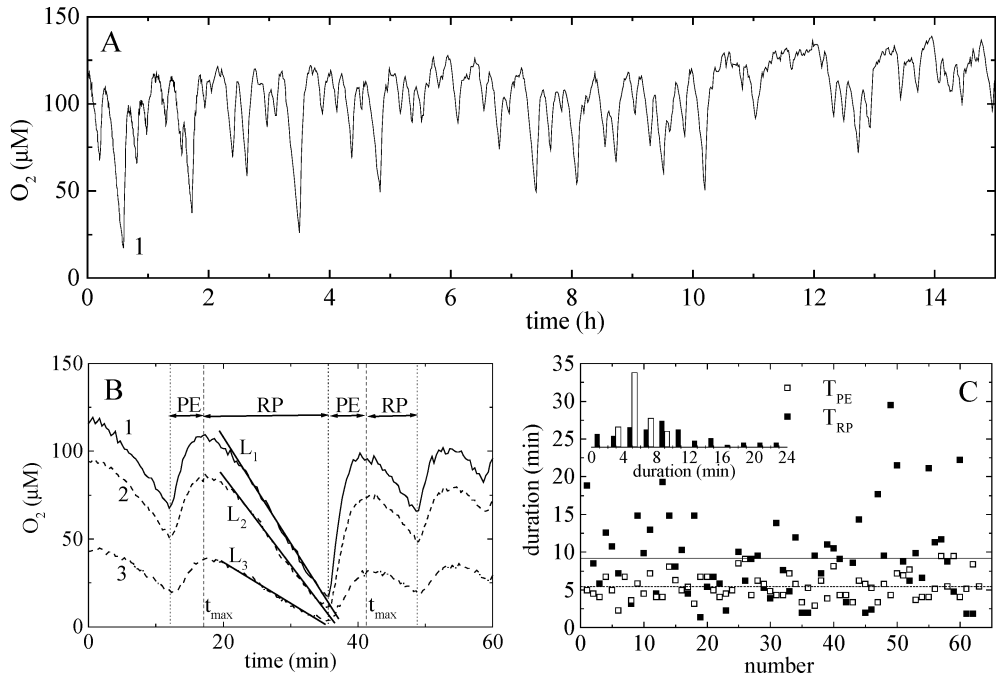

FIGURE 3. (A−B) Oxygen concentrations in selected pixels as a function of time extracted from image series taken around a stationary burrow with a larva dwelling in it (image examples shown in Figure 2F−I). Panel B represents a temporal detail (first hour) of the data shown in panel A. Locations of pixels corresponding to lines 1−3 are shown in Figure 2F. Note that the times at which the oxygen concentrations reach maxima (t_{max}) are very similar for all three lines. The slope of the linear approximations L_1-L_3 was used to quantify the rate of oxygen decrease $\partial c/\partial t$ in eq 4. (C) Durations of the subsequent pumping events (T_{PE}) and rest periods (T_{RP}) extracted from the time series shown in panel A and defined in panel B. Dashed and solid lines represent the average values for T_{PE} and T_{RP}, respectively. Histogram with the values binned in 2 min intervals is shown in the inset.

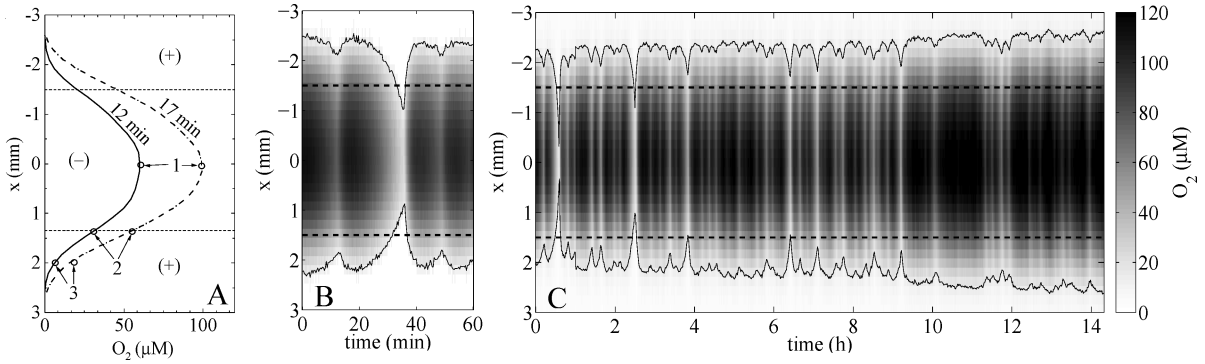

FIGURE 4. Horizontal oxygen profiles as a function of time extracted from image series taken around a stationary burrow with a larva dwelling in it (image examples shown in Figure 2F−I). The profiles were extracted along the horizontal line crossing the pixels 1−3 shown in Figure 2F. (+) and (−) in panel A indicate regions where $\partial^2 c/\partial x^2 > 0$ and $\partial^2 c/\partial x^2 < 0$, respectively. In panels B−C, the gray scale mapping of the oxygen concentrations is shown in the bar, *y*-axis represents the horizontal coordinate *x*, solid line depicts the extent of oxygen penetration X_p (see Figure 1C), dashed horizontal lines indicate the burrow diameter. Panel B represents a temporal detail (first hour) of the data shown in panel C.

less than the concentrations in selected pixels when the percentage variability (i.e., variability divided by the average value) was compared (compare Figures 3 and 4).

The volume of the oxic sediment around the burrow ($V(t)$, eq 2) and the associated oxygen uptake rate (OUB, eq 1) were calculated considering the entire oxic plume observed by the planar optode (Figure 2). The estimated average local sedimentary uptake rate $R = 63\ \mu mol\ m^{-3}\ s^{-1}$ (see above) was used in the calculation. The burrow radius was $r_0 = 1.5$ mm, the distance d between the burrow wall and the planar optode was assumed to be zero along the observed oxygen plume. Both V and OUB varied dynamically (Figure 5), which highlights the importance of the high temporal resolution measurements. The temporal variations were substantially larger during burrow construction ($V = 0-1.3$ cm^3, OUB = 0−0.29 $\mu mol\ O_2\ h^{-1}$) than around a stationary burrow ($V = 0.2-0.8$ cm^3, OUB = 0.05−0.18 $\mu mol\ O_2\ h^{-1}$). However, the corresponding averages over 14 h of observations were very similar: $V \approx 0.65$ cm^3, OUB ≈ 0.15 $\mu mol\ O_2\ h^{-1}$ (Figure 5).

Discussion

Our measurements demonstrate that oxygen distributions in the sediment around a ventilated larva burrow vary dynamically and change dramatically within minutes or even seconds. No clear spatio-temporal patterns were observed during the burrow construction period (Figure 2A−D). Once the burrow was constructed and the larva dwelled in it, the oxygen distributions became more confined in space but the temporal variations still appeared random (Figure 2F−I

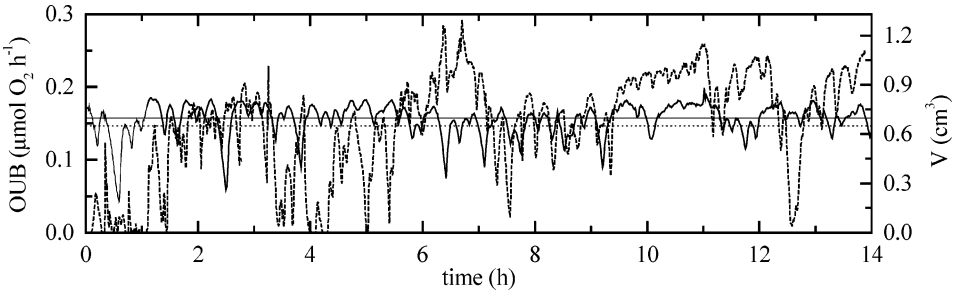

FIGURE 5. Temporal variability of the volume of oxic sediment around a ventilated burrow (V, right axis) and the corresponding sedimentary oxygen uptake rate (OUB, left axis). Dashed and solid lines were calculated from the oxygen images taken during the burrow construction and around a stationary burrow, respectively (see Figure 2 for image examples and the Supporting Information videos). Calculations were based on eqs 1−3, considering the burrow radius r_0 = 1.5 mm and assuming the distance between the burrow and the planar optode d = 0. Horizontal lines represent the corresponding time averages.

and Figure 3). These findings imply that sporadically obtained oxygen images, such as those acquired in-situ by Wenzhoefer and Glud (*15*) every 15−30 min, can be used only as an illustration of the bioirrigation effects on sediment oxygenation. Quantification of these effects is meaningful only when the 2D oxygen distributions are obtained with a much higher temporal resolution (a few seconds).

If a burrow is not directly touching the planar optode, the imaging technique is insensitive to actual burrow O_2 levels. Thus our definition of the pumping and resting periods, which is based on the response of the surrounding sediment to the O_2 oscillations inside the burrow (Figure 3), may not be strictly accurate from the animal's perspective. However, this paper is concerned only with the effects of burrow ventilation on the sediment oxygenation and thus the defined PE and RP durations are relevant temporal characteristics of the bioirrigation activity.

The high temporal resolution series of oxygen images were used to estimate the volume of the oxygenated sediment around the burrow and the associated enhancement of the sedimentary oxygen uptake rate (Figure 5). The approximate character of this quantification should be emphasized, as the model on which they were based is simplistic and does not adequately consider a few important issues. Numerical simulations (see Supporting Information 1) revealed that the oxic sediment volume derived from the planar optode measurements using eqs 2−3 (V_{+PO}) overestimates the actual volume around a burrow ventilated in the same temporal fashion but located far away from the planar optode wall (V_{-PO}). The level of overestimation varies depending on the characteristics of the sediment (R, D_s), the burrow geometry (r_0, d) and the duration of the resting periods (T_{RP}). Using a range of values close to those determined experimentally, the time-averaged V_{+PO} generally overestimates V_{-PO} by 10−20%. However, when the volumes at specific times are compared, V_{+PO} can overestimate V_{-PO} by as much as ∼120%, especially when the RP durations are long (see Figure S2 and Table S1 in the Supporting Information 1). This overestimation, which is inherent to the planar optode technique, can be qualitatively explained as the effect of the "missing sediment" and the diffusion-limited oxygen transport around the burrow during the rest period: if the burrow is located near a PO, the oxygen consumption capacity of the sediment surrounding it is lower, particularly at the PO side of the burrow. Since the O_2 transport is diffusion limited, this missing consumption capacity cannot be immediately counterbalanced by an equivalent increase of the oxic sediment volume around the burrow, as assumed in our simplified model ($M \rightarrow M'$ in Figure 1C; eq 3). This will result in a more abundant and longer lasting presence of oxygen (concentration and penetration distance) observed by the PO than would be the case without the PO.

Visual inspection of the burrow opening revealed that the burrow touched the planar optode at the sediment surface (i.e., $d = 0$ at $z = 0$). We assumed that d, which is needed for the calculation of the oxygenated sediment volume (eqs 2−3), was zero along the entire length of the oxic plume observed by the planar optode. Since this could not be checked directly without destroying the burrow, this assumption could also bias our calculations of V_{oxic}. Calculations carried out with $d = 1$ mm resulted in values ∼40% higher than those using $d = 0$.

This means that, by neglecting the missing sediment effect on one hand, the results deduced from what is observed by the planar optode can overestimate the real effects of bioirrigation on the sediment−water oxygen exchange. On the other hand, the distance between the burrow and the planar optode may be unknown or the planar optode may not "see" the effects around the entire burrow, simply because part of it is too far away from the optode. This may, in contrast, lead to underestimated quantification of the bioirrigation effects. These are serious drawbacks of the planar optode based technique that need to be satisfactorily addressed if it is to be used for more quantitative studies of bioirrigation. The problem with the "invisible" burrows could be solved by using an aquarium whose walls, each equipped with a planar optode, would be sufficiently close to each other, thus preventing the pumping animal from creating a burrow too far from either. However, whether such "confinement" influences the animal activity would have to be checked carefully. To address the missing sediment problem, a more advanced model is needed to aid more solid interpretation of the planar optode based measurements and thus provide a better estimate of the oxic sediment volume and its dynamics. It should ideally be a 3D model that would allow determination of the geometrical (e.g., the distance of the burrow from the wall) and transport-related (e.g., the local oxygen uptake rate and diffusion coefficient) parameters from the data measured by the planar optode as well as provide insights into the sensitivity of the measurements to these parameters. Solving the diffusion−advection−reaction equations using the measured time-variable boundary condition at the planar optode could be a possible approach to achieve this goal. An extension of the recently developed model by Meile et al. (*32*) by including the planar optode boundary near a burrow could be another possibility. Further research is required to explore these options.

Typical length of the oxic plumes observed by the optode was 2.8 cm (Figure 2), which corresponds to a burrow wall area of ∼2.6 cm^2. The measured time-averaged O_2 uptake rate by the sediment surrounding the burrow (OUB ∼0.15 μmol O_2 h^{-1}) can thus be translated into a time-averaged O_2 flux across the burrow wall of $J_B \approx 0.58$ mmol O_2 m^{-2} h^{-1}. This flux constitutes approximately 64% of the diffusive

oxygen flux measured at the sediment-water interface ($J_S \approx$ 0.9 mmol O_2 m^{-2} h^{-1}). It should be noted that the ratio J_B/J_S describes the relation between the amount of O_2 consumed by the sediment due to the bioirrigation-induced O_2 oscillations inside the burrow and that taken up in a stationary manner through the sediment−water interface. Since the high spatio-temporal planar optode measurements enable estimation of the temporal dynamics of this ratio, they can provide a valuable input for existing models describing the effects of burrow ventilation on biogeochemical processes in sediments (*19*, *32*, *33*).

Using literature data, the measured average oxygen uptake through the burrow walls (∼0.15 μmol O_2 h^{-1}) constitutes approximately 21−50% of the metabolic oxygen needs of a *C. plumosus* individual (0.3−0.7 μmol O_2 h^{-1}; ref *34*). The larva must therefore pump ∼21−50% more water into its burrow to sustain itself as well as to compensate for the oxygen loss due to the consumption by the sediment surrounding the burrow. It must be emphasized that this figure of merit is possibly underestimated, as it is calculated from the oxic plumes *visible* to the optode (on average 2.8 cm long; Figure 2), which is considerably shorter than the typical length of the U-shaped burrow (10−30 cm) in which the larva dwells.

In summary, we demonstrated the potential of the high temporal resolution oxygen imaging in the study of bioirrigation. Even though a more advanced model is still needed to aid more precise interpretation of the measured data, the temporal variation of the pumping activity and its effects on the oxygen exchange between the sediment and the overlying water can already be estimated using the simplified model presented here. The imaging technique allows direct observation of the oxygen dynamics in the sediment around the burrow while the animal dwells undisturbed in its natural environment, although an effect of the planar optode on its behavior cannot be completely excluded. The opportunity to manipulate the conditions to which the animal is exposed, (e.g., the content of oxygen and/or other solutes in the overlying water, temperature, food availability), the possibility to study organisms with various functional traits and the compatibility with different sediment types (e.g., muddy, sandy, high/low organic content) makes this technique a valuable alternative for the comparative study of the behavior of bioirrigating animals and exchange processes between bioirrigated sediments and the overlying water.

Acknowledgments

We would like to thank Paul Faerber and Harald Osmers for the assembly of the portable luminescence lifetime imaging system, Georg Herz and Alfred Kutsche for the construction of aquaria, and Gundula Eller for supplying animals. We are also grateful to Dirk de Beer and five anonymous reviewers for valuable comments on the manuscript. This study was supported by the Max-Planck Society and the Alfred Wegener Institute for Polar and Marine Research.

Supporting Information Available

Videos detailing O_2 dynamics in the sediment and figures showing results of numerical simulations. This material is available free of charge via the Internet at http://pubs.acs.org.

Literature Cited

(1) Aller, R.; Yingst, J. Y. Biogeochemistry of tube-dwellings: a study of the sedentary polychaete Amphirite ornata (Leidy). *J. Mar. Res.* **1978**, *41*, 299−322.
(2) Boudreau, B. P.; Marinelli, R. L. A modelling study of discontinuous biological irrigation. *J. Mar. Res.* **1994**, *52*, 947−968.
(3) Aller, R. Quantifying solute distributions in the bioturbated zone of marine sediments by defining an average micro-environment. *Geochim Cosmochim Acta* **1980**, *44*, 1955−1965.
(4) Matisoff, G.; Fisher, J. B.; Matis, S. Effects of benthic macroinvertebrates on the exchange of solutes between sediments and freshwaters. *Hydrobiologia* **1985**, *122*, 29−33.
(5) Meile, C.; Van Cappellen, P. Global estimates of enhanced solute transport in marine sediments. *Limnol. Oceanogr.* **2003**, *48*, 777−786.
(6) Meysman, F. J. R.; Galaktionov, O. S.; Middelburg, J. J. Irrigation patterns induced in permeable sediments by burrow ventilation: a case study of Arenicola marina. *Mar. Ecol. Prog. Ser.* **2005**, *303*, 195−212.
(7) Wetzel, M.; Jensen, P.; Giere, O. Oxygen/sulfide regime and nematode fauna associated with Arenicola burrows: new insights in the thiobios case. *Mar. Biol.* **1995**, *124*, 301−312.
(8) Kristensen, E. Organic matter diagenesis at the oxic/anoxic interface in coastal marine sediments, with emphasis on the role of burrowing animals. *Hydrobiologia* **2000**, *426*, 1−24.
(9) Marinelli, R. L.; Lovell, C. R.; Wakeham, S. G.; Ringelberg, D.; D. C., W. Experimental investigation of the control of bacterial community composition in macrofaunal burrows. *Mar. Ecol. Prog. Ser.* **2002**, *235*, 1−13.
(10) Altmann, D.; Stief, P.; Amann, R.; de Beer, D. Nitrification in freshwater sediments as influenced by insect larvae: Quantification by microsensors and fluorescence in situ hybridization. *Microb. Ecol.* **2004**, *48*, 145−153.
(11) Papaspyrou, S.; Gregersen, T.; Kristensen, E.; Christensen, B.; Cox, R. P. Microbial reaction rates and bacterial communities in sediment surrounding burrows of two nereidid polychaetes (Nereis diversicolor and N. virens). *Mar. Biol.* **2006**, *148*, 541−550.
(12) Revsbech, N. P.; Joergensen, B. B.; Blackburn, T. H. Oxygen in the sea bottom measured with a microelectrode. *Science* **1980**, *207*, 1355−1356.
(13) Fenchel, T. Worms burrows and oxic microniches in marine sediments: 1. Spatial and temporal scales. *Mar. Biol.* **1996**, *127*, 289−295.
(14) Glud, R. N.; Gundersen, J. K.; Roey, H.; Joergensen, B. B. Seasonal dynamics of benthic O2 uptake in a semienclosed bay: Importance of diffusion and faunal activity. *Limnol. Oceanogr.* **2003**, *48* (3), 1265−1276.
(15) Wenzhoefer, F.; Glud, R. N. Small-scale spatial and temporal variability in coastal benthic O2 dynamics: Effects of fauna activity. *Limnol. Oceanogr.* **2004**, *49* (5), 1471−1481.
(16) de Beer, D.; Wenzhoefer, F.; Ferdelman, T. G.; Boehme, S. E.; Huettel, M.; van Beusekom, J. E. E.; Boettcher, M. E.; Musat, N.; Dubilier, N. Transport and mineralization rates in North Sea sandy intertidal sediments, Sylt-Romo Basin, Wadden Sea. *Limnol. Oceanogr.* **2005**, *50* (1), 113−127.
(17) Joergensen, B. B.; Glud, R. N.; Holby, O. Oxygen distribution and bioirrigation in Arctic fjord sediments (Svalbard, Barents Sea). *Mar. Ecol. Prog. Ser.* **2005**, *292*, 85−95.
(18) Glud, R. N.; Wenzhoefer, F.; Tengberg, A.; Middelboe, M.; Oguri, K.; Kitazato, H. Distribution of oxygen in surface sediments from central Sagami Bay, Japan: In situ measurements by microelectrodes and planar optodes. *Deep-Sea Res., Part I* **2005**, *52* (10), 1974−1987.
(19) Furukawa, Y. Biogeochemical consequences of macrofauna burrow ventilation. *Geochem. Trans.* **2001**, *11*, 83−91.
(20) Kristensen, E.; Jensen, M. H.; Aller, R. Direct measurement of dissolved inorganic nitrogen exchange and denitrification in individual polychaete (Nereis virens) burrows. *J. Mar. Res.* **1991**, *49* (355−377).
(21) Smith, K. L.; Laver, M.; Brown, N. Sediment community oxygen consumption and nutrient exchange in the central and eastern North Pacific. *Limnol. Oceanogr.* **1983**, *28*, 882−898.
(22) Rasmussen, H.; Joergensen, B. B. Microelectrode studies of seasonal oxygen-uptake in a coastal sediment−role of molecular diffusion. *Mar. Ecol. Prog. Ser.* **1992**, *81* (3), 289−303.
(23) Glud, R. N.; Forster, S.; Huettel, M. Influence of radial pressure gradients on solute exchange in stirred benthic chambers. *Mar. Ecol. Prog. Ser.* **1996**, *141* (1−3), 303−311.
(24) Smith, K. L.; Glatts, R. C.; Baldwin, R. J.; Beaulieu, S. E.; Uhlman, A. H.; Horn, R. C.; Reimers, C. E. An autonomous, bottom-transecting vehicle for making long time-series measurements of sediment community oxygen consumption to abyssal depths. *Limnol. Oceanogr.* **1997**, *42* (7), 1601−1612.
(25) Holst, G.; Grunwald, B. Luminescence lifetime imaging with transparent oxygen optodes. *Sens. Actuators B* **2001**, *74* (1−3), 78−90.

(26) Precht, E.; Franke, U.; Polerecky, L.; Huettel, M. Oxygen dynamics in permeable sediments with wave-driven pore water exchange. *Limnol. Oceanogr.* **2004**, *49* (3), 693−705.
(27) Polerecky, L.; Franke, U.; Werner, U.; Grunwald, B.; de Beer, D. High spatial resolution measurement of oxygen consumption rates in permeable sediments. *Limnol. Oceanogr. Methods* **2005**, *3*, 75−85.
(28) Franke, U.; Polerecky, L.; Precht, E.; Huettel, M. Wave tank study of particulate organic matter degradation in permeable sediments. *Limnol. Oceanogr.* **2006**, *51* (2), 1084−1096.
(29) Revsbech, N. P. An oxygen microsensor with a guard cathode. *Limnol. Oceanogr.* **1989**, *34* (2), 474−478.
(30) Boudreau, B. P. The diffusive tortuosity of fine-grained unlithified sediments. *Geochim. Cosmochim. Acta* **1996**, *60*, 3139−3142.
(31) Li, Y. H.; Gregory, S. Diffusion of ions in seawater and in deep-sea sediments. *Geochim. Cosmochim. Acta* **1974**, *38*, 703−714.
(32) Meile, C.; Tuncay, K.; Cappellen, R. V. Explicit representation of spatial heterogeneity in reactive transport models: application to bioirrigated sediments. *J. Geochem. Explor.* **2003**, *78*−*79*, 231−234.
(33) Furukawa, Y.; Bentley, S. J.; Lavoie, D. L. Bioirrigation modeling in experimental benthic mesocosms. *J. Mar. Res.* **2001**, *59* (3), 417−452.
(34) Bairlein, F. The respiration of Chironomus-larvae (Diptera) from deep and shallow waters under environmental hypoxia and at different temperatures. *Arch. Hydrobiol.* **1989**, *115*, 523−536.

Received for review March 2, 2006. Revised manuscript received June 22, 2006. Accepted June 28, 2006.

ES060494L